

Architected Materials with Ultra-Low Porosity for Vibration Control

Farhad Javid, Pai Wang, Ali Shanian, and Katia Bertoldi*

Periodic porous structures provide unique opportunities to manipulate the propagation of vibrations through band gaps—frequency ranges of strong elastic wave attenuation. Yet, the gap formation requires large values of porosity and this limits the application of such structures in places where porosity is constrained by other important engineering considerations. Here, we show that such restriction can be largely relaxed by introducing a novel design, in which a single-material plate is patterned with an array of alternating crack-like pores separated by small ligaments. Our numerical and experimental results indicate that the dynamic behavior of such material architecture is fully controlled by the size of the minimum ligaments, and band gaps can exist even for very low pore volume fractions (as low as 1%).

Architected materials engineered to control and manipulate the propagation of elastic waves are attracting a growing interest because of their broad range of applications including frequency modulation,^[1] wave guiding,^[2–8] acoustic cloaking,^[9,10] wave filtering,^[11–13] and thermal management.^[14–18] The ability of these heterogeneous systems to tailor the propagation of waves originates from the existence of band gaps—frequency ranges of strong wave attenuation—which are typically induced by Bragg scattering. Bragg-type band gaps are the result of multiple scattering of waves at the interface of materials with different acoustic properties, highly depend on the periodicity and symmetry of the microstructure, and typically occur at the wavelengths of the order of the structure's unit cell size.^[19] Therefore, the formation of such gaps require a periodic structure with a high volume fraction of scatters^[20–24] with density and elastic properties significantly different from those of the matrix material.^[25,26]

Although Bragg-type band gaps have been also demonstrated in architected materials made of multiple elastic phases,^[25–29] single-material systems comprising a periodic distribution of pores have attracted most of the attention^[24,30,31] since their

monolithic design significantly facilitates the fabrication process.^[32–34] However, to form band gaps these structures need to have large values of porosity,^[22,23] a requirement that severely limits their applications, especially in those situations where specific porosities must be targeted. It is a common belief that the formation of band gaps in architected materials with low values of porosity is not feasible.

In this study, we demonstrate both numerically and experimentally that 2D periodic structures with extremely low porosities are capable of forming large band gaps. In fact, our results indicate that by altering the shape of the pores, we can manipulate the wave propagation in these systems and form band gaps even for porosities as low as 0.01. We first demonstrate the concept for a 2D structure characterized by a square array of mutually orthogonal elliptical pores and then show that the proposed mechanism is robust and can be extended to pores with different profiles, orientations, and arrangements. Importantly, we find that the presence and size of the band gaps are controlled by the smallest geometric feature in the system (which can be easily controlled by tuning the aspect ratio of the pores), providing an important guideline for the design of systems with the desired response.

We start by focusing on 2D periodic structures comprising alternating orthogonal elliptical pores arranged on a square array (see sketches in Figure 1 at right) and investigate the effect of the pore aspect ratio on their dynamic response using the commercial finite element (FE) package ABAQUS/Standard (see Methods and the Supporting Information for details of the numerical calculations). In Figure 1, we report the band diagram for three structures characterized by the same value of porosity, $\psi = \pi a b / L^2 = 0.05$ (L being the center-to-center distance between adjacent pores and a and b denoting the major and minor semiaxes of each elliptical pore, respectively), but different aspect ratios, a/b . For the conventional design with circular holes (i.e., $a/b = 1$), no band gap is observed (see Figure 1a), so waves with all frequencies can propagate through the structure. This is expected, since it is well-known that, for circular holes arranged on a square array, no band gap appears for $\psi < 0.43$.^[23,35] However, as the aspect ratio of the elliptical holes increases, we find that band gaps appear for normalized frequencies $\bar{\omega} = \omega L / (\pi c_T) < 2$ (see Figure 1b and c). In particular, for $a/b = 27$ the material is characterized by a band gap for $1.3 \leq \bar{\omega} \leq 1.34$ (between the 12th and 13th band—see Figure 1b), while for $a/b = 53$ it has two gaps, one for $0.55 \leq \bar{\omega} \leq 0.64$ (between the 8th and 9th and another for $0.78 \leq \bar{\omega} \leq 1.31$ (between the 12th and 13th band—see Figure 1c).

We then systematically study the effect of the aspect ratio of the elliptical pores, a/b , on the band gaps in extremely

Dr. F. Javid, Dr. P. Wang, Prof. K. Bertoldi
Harvard John A. Paulson School of Engineering
and Applied Sciences
Harvard University
Cambridge, MA 02138, USA
E-mail: bertoldi@seas.harvard.edu

Dr. A. Shanian
Siemens ADGT
9545 Cote de Liesse, Dorval, Québec H9P 1A5, Canada

Prof. K. Bertoldi
Kavli Institute
Harvard University
Cambridge, MA 02138, USA

DOI: 10.1002/adma.201600052



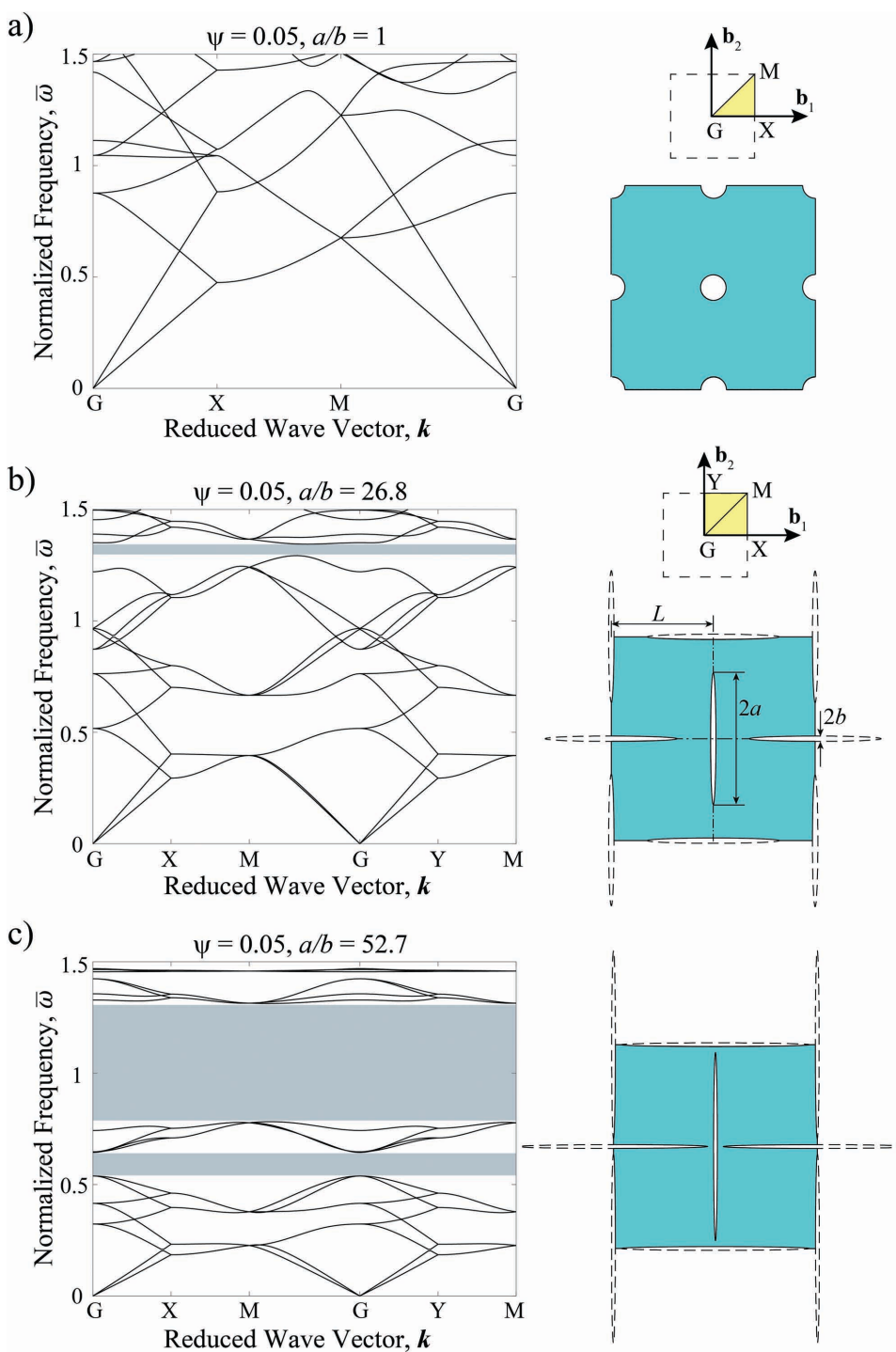


Figure 1. Band structures of periodic materials with the same porosity, $\psi = 0.05$, but different pore aspect ratios. a) Circular pores ($a/b = 1$). b) Elliptical pores characterized by $a/b = 26.8$. c) Elliptical pores characterized by $a/b = 52.7$. The gray-shaded regions indicate the band gaps. Note that because of the rotational symmetries observed in one quarter of the unit cell, the bands in the GY and YM directions are identical to those in the GX and XM directions.

low-porosity periodic materials. As shown in Figure 2a, when the porosity is fixed to be $\psi = 0.01$, a gap opens at $a/b = 128$ and widens monotonically by increasing a/b . Moreover, for $a/b > 190$ an additional gap opens at a lower frequency range. Similar evolutions of the band gaps with respect to the pores aspect

ratio, a/b , are observed for different values of porosity, $\psi = 0.05$ and 0.10 (see Figure 2a). However, depending on porosity, the gaps are formed at different ranges of aspect ratios (i.e., at $a/b = 24$ and 36 for $\psi = 0.05$ and at $a/b = 11$ and 17 for $\psi = 0.10$). Remarkably, as shown in Figure 2b, the frequency ranges of

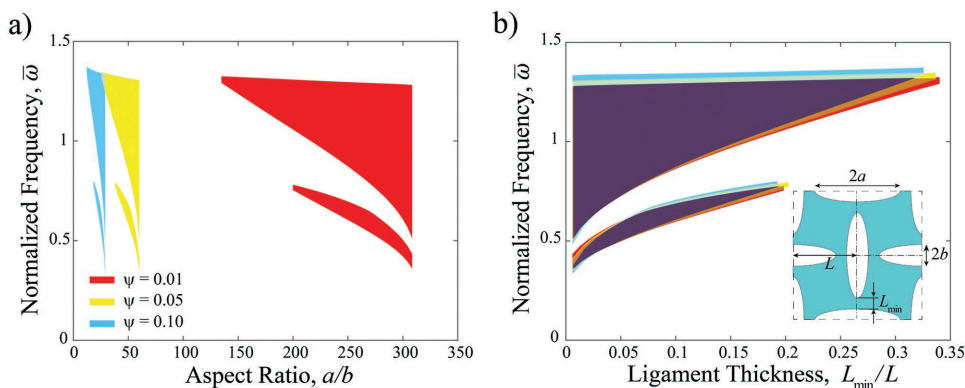


Figure 2. Evolution of band gaps with respect to geometric parameters. a) The band gaps are plotted as a function of the pores aspect ratio, a/b , for three different values of porosity ($\psi = 0.01, 0.05$, and 0.10). b) The band gaps are plotted as a function of the minimum ligament thickness, L_{\min} , for the same values of porosity ($\psi = 0.01, 0.05$, and 0.10). Remarkably, all data collapse onto each other in (b), indicating that the ligament thickness is the critical parameter that determines the dynamic response of these materials. The dark-shaded region indicates the collapsing gaps.

gaps for different porosities collapse onto each other when plotted versus the minimum thickness of the ligaments separating neighboring holes (see inset in Figure 2b)

$$L_{\min} = L - a - b = L \left[1 - \left(1 + \frac{a}{b} \right) \sqrt{\frac{\psi b}{\pi a}} \right] \quad (1)$$

This reveals that the minimum ligament thickness, L_{\min} , is the essential parameter that controls the dynamic response of these structures and that can be used to effectively design low porosity systems with the desired frequency band gaps. To explain the

crucial role played by L_{\min} , we note that the proposed architected material can be idealized as a 2D array of alternating small (corresponding to the thin ligaments of width L_{\min}) and large (corresponding to the square regions surrounded by the elongated holes) masses coupled by springs. This is a system typically studied in solid-state physics^[36,37] and it is known to result in a band gap that arises from the existence of modes of oscillation with widely different frequencies. Traveling phonon modes where the large masses are predominantly excited are split in frequency from those where the small masses are predominantly excited. Importantly, the frequency band gap

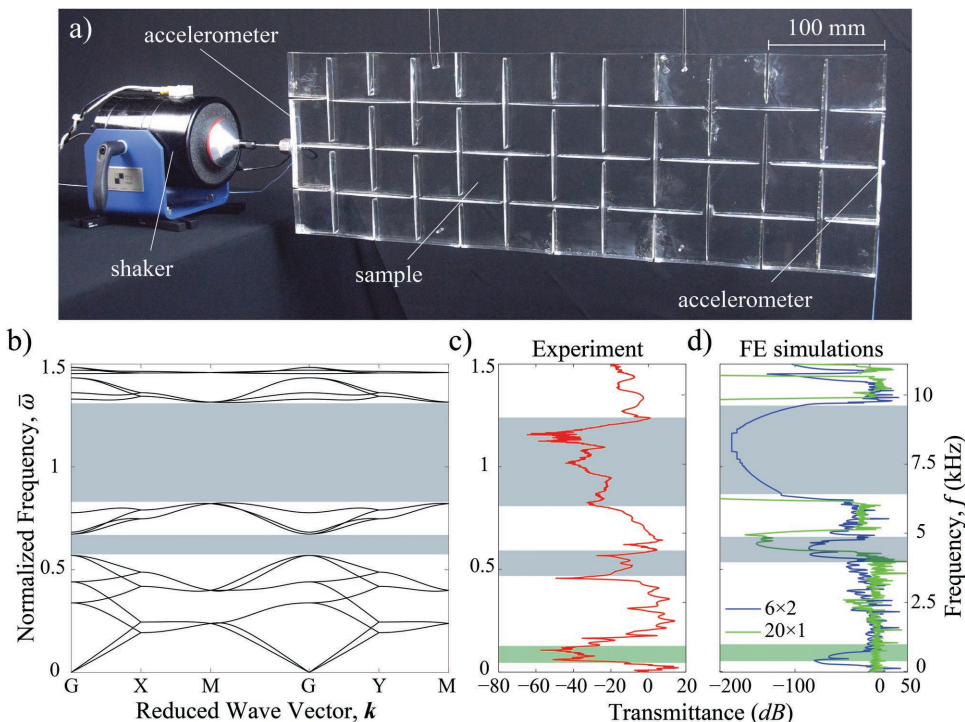


Figure 3. Experimental results. a) Experimental setup showing the sample (suspended from top), the shaker and the input/output accelerometers. b) Numerical dispersion relation from unit cell calculation. c) Experimentally measured transmittance curve for elastic waves propagating along the GX direction. d) Numerically calculated transmittance curve for elastic waves propagating along the GX direction. Two different finite-size models are considered: (i) a numerical model with the same size as the fabricated sample (blue line) and (ii) a larger model consisting of a single row of 20 unit cells and periodic boundary conditions on the lateral faces (green line).

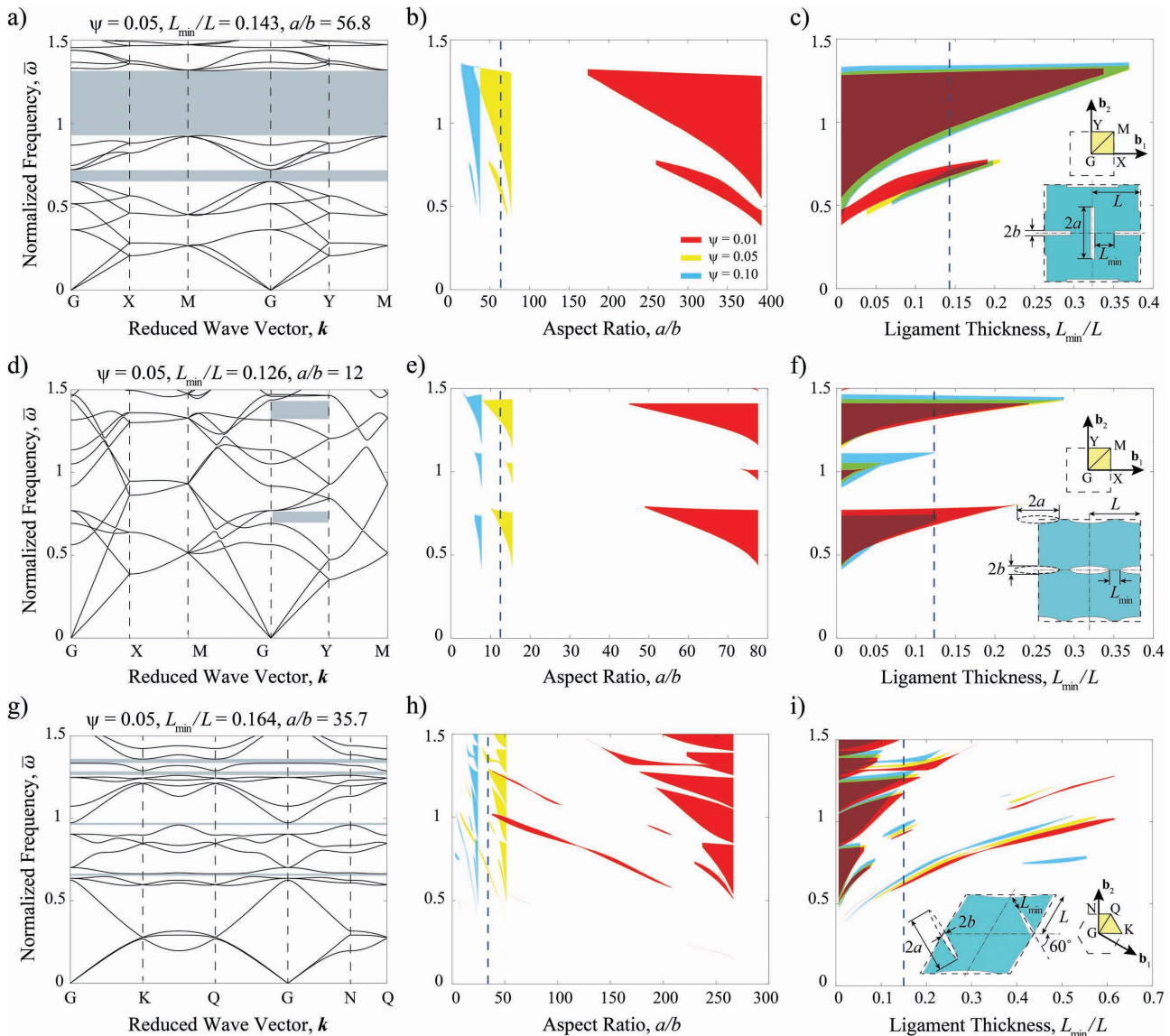


Figure 4. Effect of pores' profile, orientation, and arrangement on the band structure of low porosity periodic structures: a–c) square array of mutually orthogonal elongated rectangular pores; d–f) square array of elongated elliptical pores aligned in horizontal direction; and g–i) Kagome-like lattice of elongated elliptical pores. For all the three geometries, we report a typical dispersion relation (a,d,g), the evolution of the band gaps as function of the pores' aspect ratio, a/b (b,e,h), and the evolution of the band gaps as function of the minimum ligament thickness, L_{\min} (c,f,i). The dark-shaded regions in c,f,i sections indicate the collapsing gaps.

between low and high frequency vibrations is controlled by the ratio between the small and large masses and thus by L_{\min} in our architected material (see Supporting Information for more details).

Next, to confirm the numerical predictions, we experimentally test the dynamic response of a periodic material with $\psi = 0.048$ and $a/b = 52.9$ arranged on a 6×2 square lattice (see Figure 3a) (see the Methods for details of the experiments). The comparisons between numerical results and experimental measurements are shown in Figure 3b–d, where we report the dispersion relation from unit cell calculation (Figure 3b) and the transmittance (defined as the ratio between the output and the input acceleration signals, $\|A_{\text{out}}(\omega)/A_{\text{in}}(\omega)\|$) obtained from both experiments (Figure 3c) and finite-size FE simulations

(Figure 3d) (see Supporting Information for details of the finite-size FE simulations).

Focusing on the experimental results (Figure 3c), we find that the transmittance measured along the GX direction drops ~ 40 dB in three frequency ranges, $f = 0.3 - 1.2$ kHz, 3.25 – 4.4 kHz, and 5–9 kHz (corresponding to $0.04 \leq \bar{\omega} \leq 0.18$, $0.44 \leq \bar{\omega} \leq 0.6$, and $0.69 \leq \bar{\omega} \leq 1.2$). While the higher two attenuated frequency ranges clearly correspond to the numerically predicted band gaps, no signature of the lowest one is found in the dispersion relation (see Figure 3b). To understand this discrepancy, we numerically investigate the effect of the sample size by calculating the steady-state dynamic responses of different finite-size models (see Supporting Information for more details). While for the model with the same size

as in experiment we observe all three drops in transmittance (see blue curve in Figure 3d), the lowest one is found to disappear when we consider larger model sizes (see green curve in Figure 3d). This clearly indicates that such attenuation is caused by finite-size effects, such as the reflected waves from the boundaries. Importantly, by comparing the results obtained from models of different sizes we can distinguish boundary effects from bulk properties. In addition, we should note that, although numerical results and experimental measurements are generally in agreement for the higher two drops, these attenuation ranges are slightly shifted toward lower frequencies in experiment. This is mainly due to manufacturing inaccuracies in the laser cutting process. In fact, because of the divergence of the laser beam, the size of the pores increases through the thickness of the acrylic sheet, resulting in a smaller ligament size and, therefore, lower gap frequencies.

While the results reported so far are obtained for periodic materials with a square array of mutually orthogonal elliptical pores, we now demonstrate that the proposed mechanism is robust and can be also extended to elongated pores with different profiles, orientations, and arrangements. To this end, in Figure 4a–c, we present results for a material made of a square array of mutually orthogonal pores with rectangular profiles (see inset in Figure 4c). The dispersion plot (Figure 4a) shows that this structure is also characterized by two complete band gaps for low values of porosity ($\psi = 0.05$) if the rectangular holes have a large enough length over width ratio ($a/b > 47$). Moreover, we find that, while the band gaps appear at different values of a/b for structures with different porosities (Figure 4b), they collapse on each other if plotted versus the minimum ligament thickness (see Figure 4c and Figure S6 in Supporting Information), confirming the crucial role played by L_{\min} . Next, to investigate the effect of the pore orientation, we numerically study the dynamic response of a square array of elliptical holes all arranged horizontally (see Figure 4d–f). Since the wide horizontal strips of elastic material act as pathways which easily let the waves propagate in GX direction, only directional band gaps in GY direction are observed. However, we find that such directional gaps are also retained for low values of porosity, ψ , and that the gaps sizes are controlled by L_{\min} (Figure 4e,f). Finally, we consider elongated elliptical pores arranged on a hexagonal array to form a kagome-like pattern (see Figure 4g–i) and observe that, even in this case, at low values of porosity the system is characterized by full band gaps, whose sizes are controlled by the minimum ligament thickness (see Supporting Information for additional results).

In this study, we introduced a new class of periodic materials comprising a periodic array of elongated crack-like pores embedded in an elastic matrix and found that this design results in the formation of Bragg-type band gaps even for ultra-low values of porosity. Interestingly, our results indicate that the frequency ranges of the band gaps are not affected by the porosity, but are fully controlled by the minimum ligament thickness between adjacent pores. Finally, we demonstrated that the proposed mechanism works universally for a wide range of pores' profiles, orientations, and arrangements, providing an important guideline for the design of smart systems with targeted dynamic behavior.

Methods

Numerical Analysis: Dynamic response of the structures are numerically evaluated using the commercial FE package ABAQUS/Standard. In particular, we construct 2D models of the unit cells with triangular plain strain quadratic elements (Abaqus element type CPE6) and model the material as linear elastic with Young's modulus of $E = 1750$ MPa and Poisson's ratio of $\nu = 0.35$ (so that the elastic wave speeds are $c_T = 743\text{--}m\text{s}^{-1}$ and $c_L = 1546\text{--}m\text{s}^{-1}$ for shear and pressure waves, respectively). We then apply Bloch-type boundary conditions to the edges of the unit cell^[35,38–40] and calculate the dispersion relation $\omega = \omega(k)$ using the frequency domain perturbation technique (see Supporting Information for details on the wave propagation analysis).

Experiments: To confirm the numerical results, the dynamic response of a periodic material with $\psi = 0.048$ comprising 48 mutually orthogonal elliptical pores with $a/b = 52.9$ arranged on a 6×2 square lattice is experimentally evaluated. The specimen consists of an acrylic plate (Height \times Width \times Thickness = $200 \times 600 \times 18.2$ mm) perforated by elliptical pores with major and minor semiaxes of $a = 45.0$ mm and $b = 0.85$ mm (see Figure 3a) using a commercial laser cutter (KT150, Kern Laser Systems). During the dynamic tests the sample is suspended in air and is vibrated by an electrodynamic shaker (K2025E013, Modal Shop), which provides a white noise input signal over a broadband frequency range. Two miniature accelerometers (352C22, PCB Piezotronics) are attached to both ends of the sample (one exactly above the shaker tip and the other one at the opposite end of the specimen—see Figure 3a) to measure the transmittance of the sample versus the frequency of the incident wave.

Supporting Information

Supporting Information is available from the Wiley Online Library or from the author.

Acknowledgements

This work has been funded by Siemens ADGT. The authors also acknowledge support by the Materials Research Science and Engineering Center under National Science Foundation (NSF) Award No. DMR-1420570, NSF CMMI-1149456-CAREER award, and the support of the Kavli Institute at Harvard University. The authors thank Prof. David R. Clarke, Stan Cottreau, Sahab Babaee, Sijie Sun and Vincent Tourant for inspirational discussions and their help in performing the experiments. The authors declare that they have no competing financial interests.

Received: January 5, 2016

Revised: March 7, 2016

Published online:

- [1] W. Cheng, J. J. Wang, U. Jonas, G. Fytas, N. Stefanou, *Nat. Mater.* **2006**, *5*, 830.
- [2] M. Kafesaki, M. M. Sigalas, N. Garcia, *Phys. Rev. Lett.* **2000**, *85*, 4044.
- [3] A. Khelif, A. Chouja, S. Benchabane, B. Djafari-Rouhani, V. Laude, *Appl. Phys. Lett.* **2004**, *84*, 4400.
- [4] D. Elser, U. L. Anderson, A. Korn, O. Glöckl, S. Lorenz, Ch. Marquardt, G. Leuchs, *Phys. Rev. Lett.* **2006**, *97*, 133901.
- [5] J. O. Vasseur et al., *J. Appl. Phys.* **2007**, *101*, 114904.
- [6] Y. Pennec et al., *Phys. Rev. B* **2009**, *80*, 144302.
- [7] A. Cebrecos et al., *J. Phys. D: Appl. Phys.* **2015**, *48*, 025501.
- [8] J. Sun, T. Wu, *Phys. Rev. B* **2007**, *76*, 104304.
- [9] S. A. Cummer, D. Schurig, *New J. Phys.* **2007**, *9*, 45.
- [10] H. Chen, C. T. Chan, *Appl. Phys. Lett.* **2007**, *91*, 183518.

- [11] T. Elnady et al, *Appl. Phys. Lett.* **2009**, *94*, 134104.
- [12] M. M. Sigalas, *J. Appl. Phys.* **1998**, *84*, 3026.
- [13] Z. J. Yao, G. L. Yu, Y. S. Wang, Z. F. Shi, *Int. J. Solids Struct.* **2009**, *46*, 2571.
- [14] S. Narayana, Y. Sato, *Phys. Rev. Lett.* **2012**, *108*, 214303.
- [15] R. Schittny, M. Kadic, S. Guenneau, M. Wegener, *Phys. Rev. Lett.* **2013**, *110*, 195901.
- [16] M. Maldovan, *Phys. Rev. Lett.* **2013**, *110*, 025902.
- [17] B. L. Davis, M. I. Hussein, *Phys. Rev. Lett.* **2014**, *112*, 055505.
- [18] L. Yang, N. Yang, B. Li, *Nano Letters* **2014**, *14*, 1734.
- [19] M. Maldovan, *Nature* **2013**, *503*, 209.
- [20] M. Kushwaha, B. Djafari-Rouhani, *J. Sound Vibrat.* **1998**, *218*, 697.
- [21] X. Zhang, Z. Liu, Y. Liu, F. Wu, *Phys. Lett. A* **2003**, *313*, 455.
- [22] Y. Liu, J.-Y. Su, L. Gao, *Phys. Lett. A* **2008**, *372*, 6784.
- [23] M. Maldovan, E. Thomas, *Appl. Phys. B* **2006**, *83*, 595.
- [24] J. O. Vasseur, P. A. Deymier, B. Djafari-Rouhani, Y. Pennec, A.-C. Hladky-Hennion, *Phys. Rev. B* **2008**, *77*, 085415.
- [25] Z. Liu, C. T. Chan, P. Sheng, *Phys. Rev. B* **2002**, *65*, 165116.
- [26] M. S. Kushwaha, P. Halevi, G. Martínez, L. Dobrzynski, B. Djafari-Rouhani, *Phys. Rev. B* **1994**, *49*, 2313.
- [27] M. Sigalas, E. Economou, *Solid State Commun.* **1993**, *86*, 141.
- [28] M. S. Kushwaha, P. Halevi, L. Dobrzynski, B. Djafari-Rouhani, *Phys. Rev. Lett.* **1993**, *71*, 2022.
- [29] A. Khelif, B. Aoubiza, S. Mohammadi, A. Adibi, V. Laude, *Phys. Rev. E* **2006**, *74*, 046610.
- [30] Y. Tanaka, Y. Tomoyasu, S.-I. Tamura, *Phys. Rev. B* **2000**, *62*, 7387.
- [31] T. Gorishnyy, C. K. Ullal, M. Maldovan, G. Fytas, E. L. Thomas, *Phys. Rev. Lett.* **2005**, *94*, 115501.
- [32] J. Jang et al, *Adv. Funct. Mater.* **2007**, *17*, 3027.
- [33] R. H. Olsson III, I. El-Kady, *Meas. Sci. Technol.* **2009**, *20*, 012002.
- [34] M. Eichenfield, J. Chan, R. M. Camacho, K. J. Vahala, O. Painter, *Nature* **2009**, *462*, 78.
- [35] M. Maldovan, E. Thomas, *Periodic Materials and Interference Lithography: For Photonics, Phononics and Mechanics*, Wiley-VCH, Weinheim, Germany **2009**.
- [36] C. Kittel, *Introduction to Solid State Physics*, 6th ed., John Wiley, New York, **1986**.
- [37] A. H. Safavi-Naeini, O. Painter, *Opt. Express* **2010**, *18*, 14926.
- [38] F. Bloch, *Z. Phys.* **1929**, *52*, 555.
- [39] L. Brillouin, *Wave Propagation in Periodic Structure*, McGraw-Hill, New York **1946**.
- [40] P. Wang, J. Shim, K. Bertoldi, *Phys. Rev. B* **2013**, *88*, 014304.

Copyright WILEY-VCH Verlag GmbH & Co. KGaA, 69469 Weinheim, Germany, 2016.

ADVANCED MATERIALS

Supporting Information

for *Adv. Mater.*, DOI: 10.1002/adma.201600052

Architected Materials with Ultra-Low Porosity for Vibration Control

*Farhad Javid, Pai Wang, Ali Shanian, and Katia Bertoldi**

Supplementary Information for Architected Materials with Ultra-low Porosity for Vibra- tion Control

Farhad Javid,¹ Pai Wang,¹ Ali Shanian,² and Katia Bertoldi^{1,3*}

¹*John A. Paulson School of Engineering and Applied Sciences, Harvard University, Cambridge, Massachusetts, 02138, USA.*

²*Siemens ADGT, 9545 Cote de Liesse, Dorval, Québec, H9P 1A5, Canada.*

³*Kavli Institute, Harvard University, Cambridge, Massachusetts, 02138, USA.*

*Corresponding Author. Tel: +1 617 496 3084; E-mail: bertoldi@seas.harvard.edu

S1 Wave propagation analysis

Bloch wave analysis for infinitely large periodic structures: The propagation of mechanical waves within infinitely large porous materials is investigated numerically by considering 2D periodic unit cells spanned by the lattice vectors $\mathbf{a}_1 = [2L, 0]$ and $\mathbf{a}_2 = [0, 2L]$, as shown in Fig. S1a. The reciprocal lattice is identified by the reciprocal lattice vectors

$$\mathbf{b}_1 = 2\pi \frac{\mathbf{a}_2 \times \mathbf{z}}{\|\mathbf{z}\|^2}, \quad \mathbf{b}_2 = 2\pi \frac{\mathbf{z} \times \mathbf{a}_1}{\|\mathbf{z}\|^2} \quad (\text{S1})$$

satisfying $\mathbf{a}_i \cdot \mathbf{b}_j = 2\delta_{ij}$, where δ_{ij} is the Kronecker delta and $\mathbf{z} = \mathbf{a}_1 \times \mathbf{a}_2$.

In order to obtain the dispersion relation of the propagating waves in the porous system, frequency domain wave propagation analyses are performed on the unit cell. Bloch-type boundary

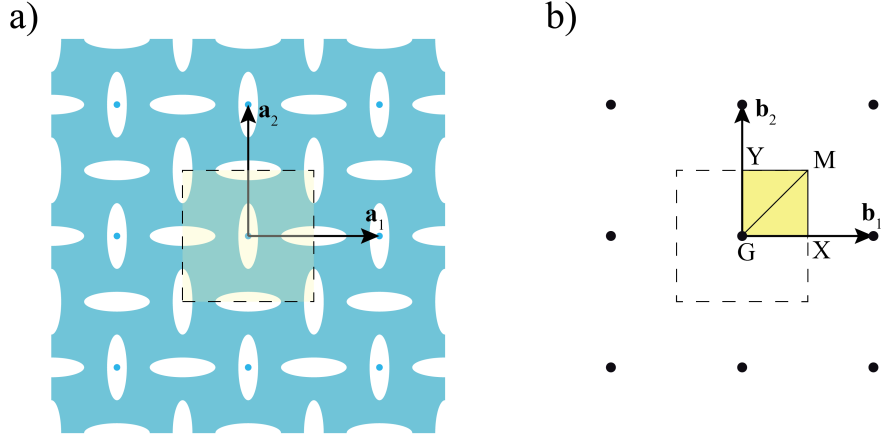


Figure S1: (a) The 2D periodic structure spanned by the lattice vectors $\mathbf{a}_1 = [2L, 0]$ and $\mathbf{a}_2 = [0, 2L]$. A unit cell of this structure is highlighted in yellow. (b) Corresponding reciprocal lattice (black dots) and first Brillouin zone (yellow area) in the reciprocal space.

conditions¹ of the form

$$\mathbf{u}(\mathbf{x} + \mathbf{r}) = \mathbf{u}(\mathbf{x}) \exp(i\mathbf{k} \cdot \mathbf{r}), \quad (\text{S2})$$

are applied to the edges of the unit cell, where \mathbf{u} and \mathbf{x} denote, respectively, the displacement and position vector of a point. Moreover, \mathbf{r} is the distance between each pair of nodes periodically located on the boundaries and \mathbf{k} is Bloch-wave vector. Since most commercial finite element packages do not support the complex-valued displacements introduced by Eq. (S2), following Aberg and Gudmundson², we split any complex-valued spatial function $\phi(\mathbf{x})$ into a real and an imaginary part

$$\phi(\mathbf{x}) = \phi(\mathbf{x})^{re} + i\phi(\mathbf{x})^{im}. \quad (\text{S3})$$

The problem is then solved using two identical finite element meshes for the unit cell, one for the

real part and the other for the imaginary part, coupled by

$$\mathbf{u}^{re}(\mathbf{x} + \mathbf{r}) = \mathbf{u}^{re}(\mathbf{x}) \cos(\mathbf{k} \cdot \mathbf{r}) - \mathbf{u}^{im}(\mathbf{x}) \sin(\mathbf{k} \cdot \mathbf{r}), \quad (\text{S4})$$

and

$$\mathbf{u}^{im}(\mathbf{x} + \mathbf{r}) = \mathbf{u}^{re}(\mathbf{x}) \sin(\mathbf{k} \cdot \mathbf{r}) + \mathbf{u}^{im}(\mathbf{x}) \cos(\mathbf{k} \cdot \mathbf{r}). \quad (\text{S5})$$

Note that Eqs. (S4) and (S5) are implemented into Abaqus/Standard via multi-point constraints ³.

Focusing on the propagation of small amplitude waves, we calculate the dispersion relation $\omega = \omega(\mathbf{k})$ using the frequency domain perturbation method. In particular, the dispersion band diagrams reported in this work (e.g., see Figs. 1 and 3b) is obtained by choosing \mathbf{k} on the perimeter of the *irreducible Brillouin zone* ^{3–5} (yellow triangle in Fig. S1b) and considering 32 uniformly-spaced points along each edge.

Steady-state dynamic analysis for finite-size structures: The dynamic response of finite-sized structures in the main text is investigated numerically by calculating their steady-state dynamic response to harmonic excitations. As shown in Fig. S2, two finite size 2D models, one consisting of 6×2 unit cells and the other consisting of 20×1 unit cells with periodic boundary conditions on the horizontal edges, are constructed using Abaqus triangular plain strain quadratic elements (Abaqus element type CPE6). The first model is identical to the experimental sample, while the second one is used to study how boundary effects affect the dynamic response of the structure.

The material is modeled as linear elastic with Young's modulus of $E = 1750$ MPa (as for the acrylic sheet used in experiments) and Poisson's ratio of $\nu = 0.35$. A linear perturbation steady-

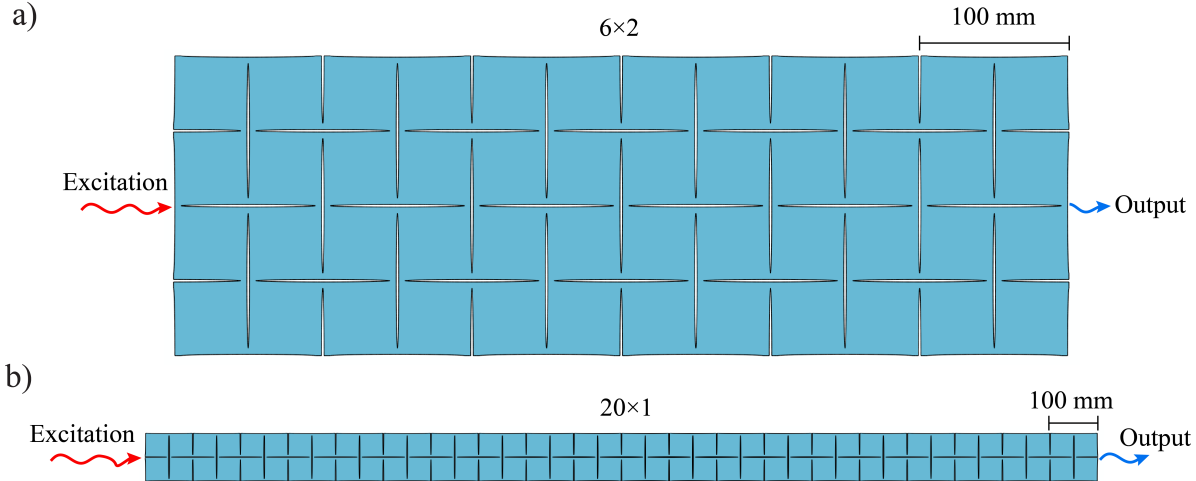


Figure S2: Finite-sized 2D models used for the steady-state dynamic analysis: (a) model comprising 6×2 unit cells; (b) model comprising 20×1 unit cells. Periodic boundary conditions are applied to the horizontal edges.

state dynamics analysis is performed on each model for the frequency range of $\omega = 0 - 12000$ Hz. To this end, an excitation is applied to one end of the models and the output is measured at the other end (see Fig. S2).

S2 The role of the minimum ligament thickness

The results presented in the main text reveal that the minimum ligament thickness, L_{\min} , is the essential parameter that controls the dynamic response of the proposed structures. To explain the crucial role played by L_{\min} , we note that the proposed architected material can be idealized as a 2D array of alternating small (corresponding to the thin ligaments of width L_{\min}) and large (corresponding to the square regions surrounded by the elongated holes) masses coupled by springs. As shown in Fig. S3, when L_{\min} decreases (by increasing the aspect ratio of the elliptical holes while keeping the porosity constant), the mass m_2 associated to the thin ligaments monotonically decreases, while the mass m_1 associated to the square regions slightly increases. As a result, the mass ratio m_1/m_2 monotonically increases and this is known to lead to a band gap that arises from the existence of modes of oscillation with widely different frequencies^{6,7}. For the sake of simplicity, here we consider a simple 1D system composed of two concentrated masses, m_1 and m_2 connected by springs of stiffness k_0 . For such system, the two branches of the dispersion relation are given by

$$\omega_{1,2}^2 = \omega_0^2 \pm \sqrt{\omega_0^4 - \frac{4k_0^2}{m_1 m_2} \sin^2 kL}, \quad \text{where} \quad \omega_0^2 = k_0 \left(\frac{1}{m_1} + \frac{1}{m_2} \right) \quad (\text{S6})$$

where k is the reduced wave vector (note that for this 1D system the wave vector is a scalar). In Fig. S3b we plot the dispersion relation for a diatomic chain with $m_1/m_2 = 1, 2$ and 10 . We see that large band gaps exist in this structure as m_1/m_2 is increased, just as in the porous material considered in this study.

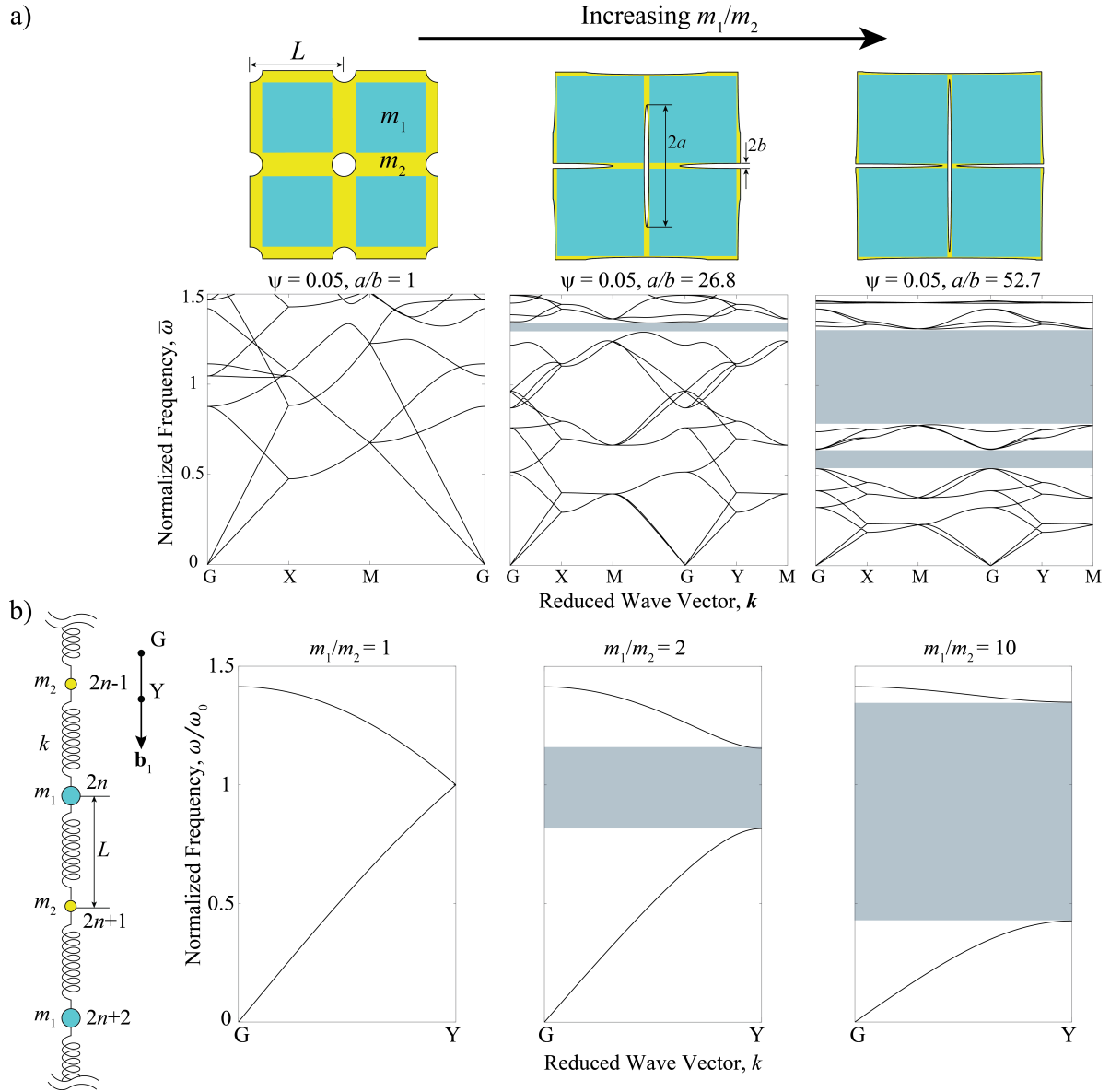


Figure S3: a) In the porous structures the mass ratio m_1/m_2 increases as the minimum ligament thickness, L_{\min} , decreases. This leads to the opening and widening of a band gap. b) A similar behavior is observed in a 1D mass-spring system.

S3 Additional Numerical Results

Effect of Porosity in Periodic Materials with Circular Pores In Fig. S4, we plot the dispersion relation for a square array of circular pores in a 2D elastic material for three different values of porosity ($\psi = 0.7, 0.55$, and 0.4). As expected, the results indicate that, as the porosity is reduced, the width of the band gap progressively decreases. In particular, we find that for $\psi = 0.4$ no band gap for low ranges of frequency ($\bar{\omega} = \omega L / (\pi c_T) < 2$) is formed. These results fully agree with previous calculations indicating that in 2D structures perforated with a square array of circular pores bandgaps are suppressed for $\psi < 0.43^{8,9}$.

Effect of Pores' Profile and Orientation To further demonstrate the robustness of the proposed concept, here we present additional results for periodic materials with different pores' profile and orientations. In particular, in Fig. S5a-c we focus on a square array of mutually orthogonal elongated rectangular pores with rounded tips (see inset in Fig. S5c). The dispersion plot shows that, if the pores have a large enough aspect ratio, this structure is also characterized by two band gaps for $\psi = 0.05$. Moreover, similar to the cases reported in Fig. 4, the band gaps of structures with different porosities appear in different aspect ratio ranges (see Fig. S5b) but they collapse on a single curve if plotted versus the minimum ligament thickness (see Fig. S5c).

Next, in Figs. S5d-f and g-i we study the effect of pores orientation and consider structures with elongated elliptical pores oriented to form a "X" pattern (see inset in Fig. S5f) and a zig-zag pattern (see inset in Fig. S5i). Again, for the "X"-pattern structure we find band gaps even for low values of porosity (Figs. S5d) which are appeared in different pores' aspect ratio ranges (Figs. S5e)

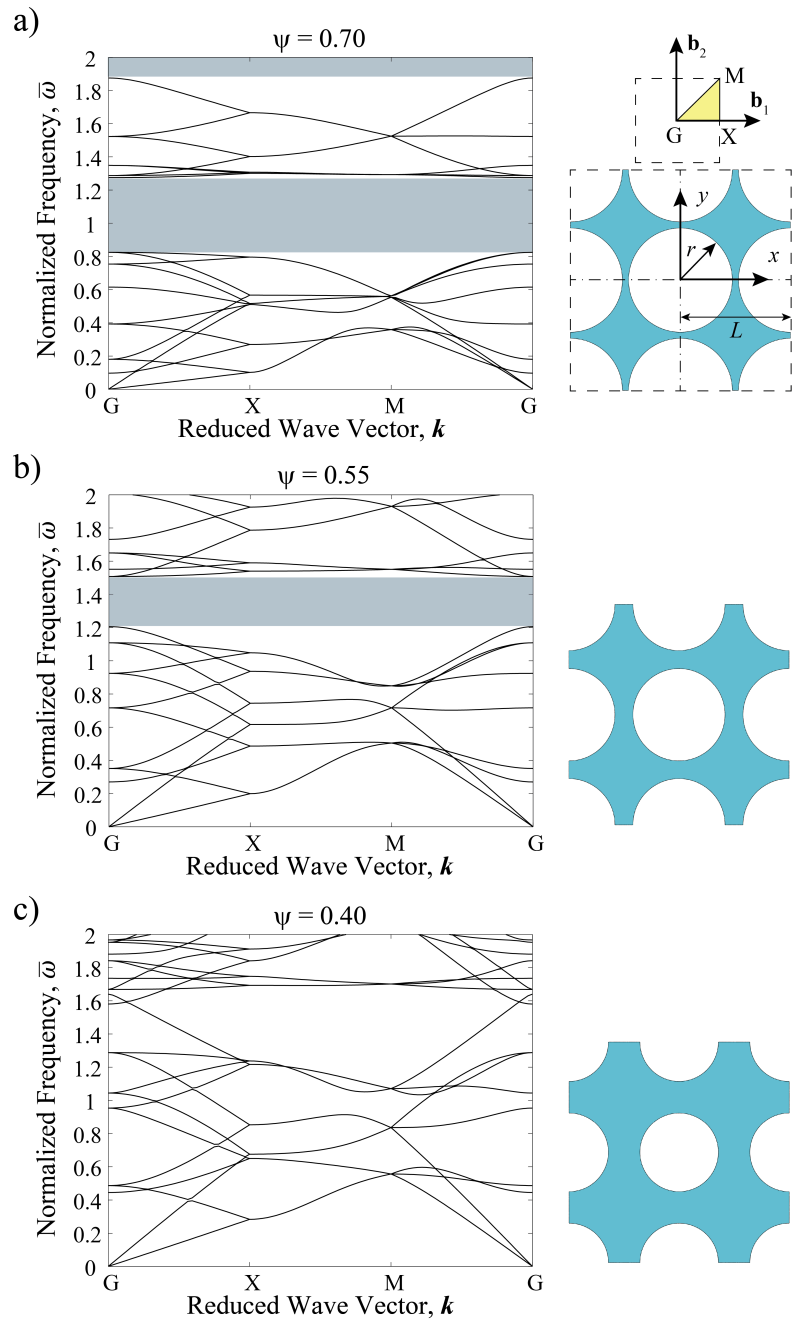


Figure S4: Dispersion relation for a square array of circular pores in a 2D elastic sheet: a) $\psi = 0.7$, b) $\psi = 0.55$, and c) $\psi = 0.4$.

but they all collapse on each other when plotted versus L_{\min} (Fig. S5f). For the structure with the zig-zag pattern only directional band gaps are observed since the minimum ligament thickness only affects the wave propagation in vertical directions (Fig. S5i). However, similar to the previous cases, the minimum ligament thickness is found to be the governing parameter that controls the band gaps behavior in this structure.

Effect of Pores' Sharpness Finally, in Fig. S6 we plot the frequency ranges of gaps versus the minimum thickness of the ligaments separating neighboring holes for periodic materials with a square array of mutually orthogonal rectangular, oval, elliptical and rhombic pores, all characterized by the same porosity ($\psi = 0.05$). Importantly, we find that the band gaps of all the four structures collapse on each other, proving that the effect of the pores profile is minimal.

Effect of Sample Thickness While all numerical analysis presented in this study were conducted under plane strain assumptions, to study the effect of the sample thickness we also considered the extreme case of a very thin model constructed using shell elements. As shown in Fig. S7, the band gaps of the thin 6×2 model are very similar to those of the corresponding plane strain one, indicating that the dynamic response of the architected material is not significantly affected by the thickness of the structure.

Effect of Boundaries The choice of origin for "cutting out" a finite sample is always arbitrary, and any boundary effect will be largely determined by this choice. However, we expect the bulk properties of the architected material not to be affected by this. To demonstrate this point, in Fig. S8 we show results obtained from two 6×2 structures with original and half-length ($0.5L$) edge

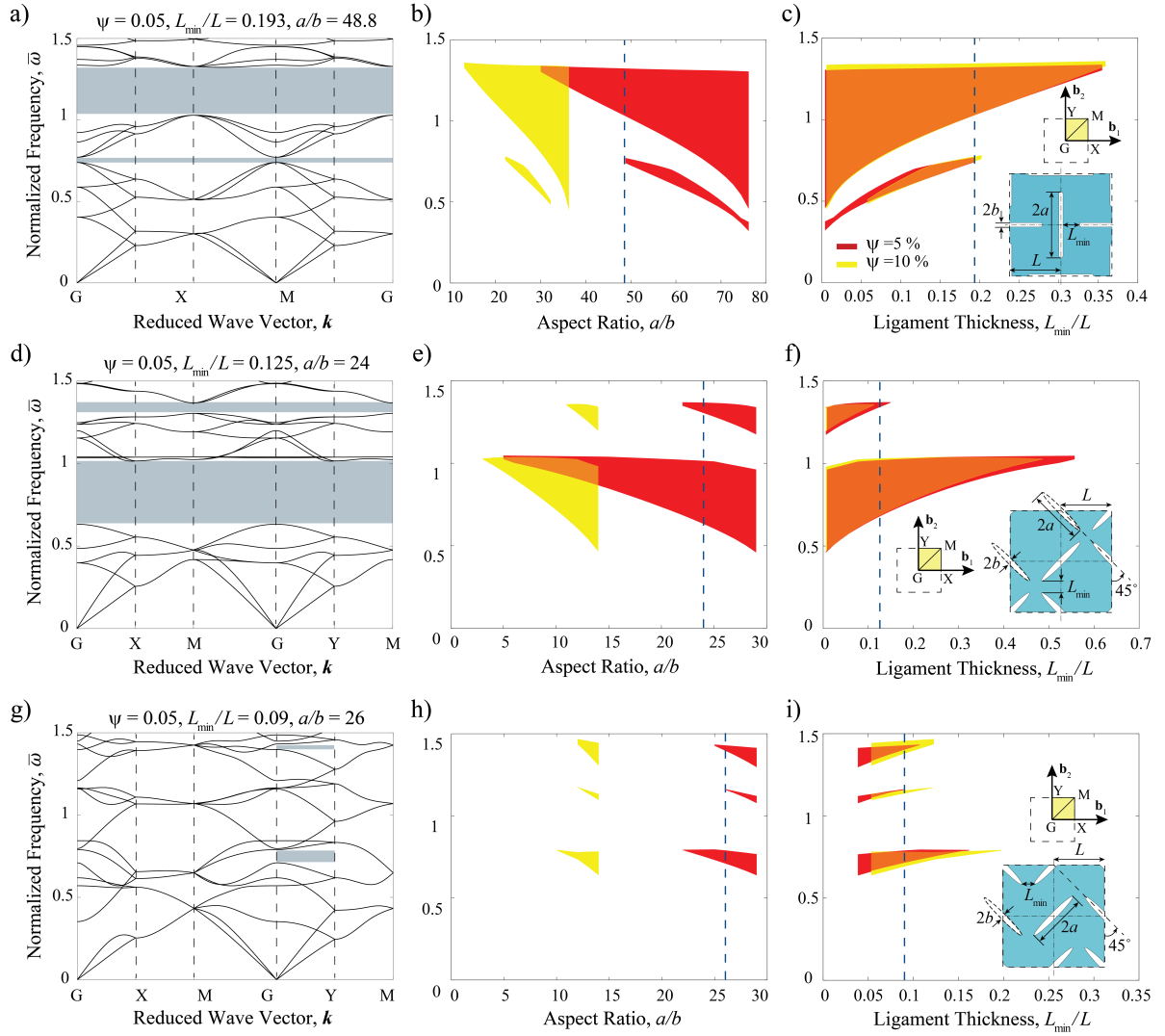


Figure S5: Effect of the pores' profile and orientation on the band structure of the periodic materials: (a-c) Square array of mutually orthogonal elongated rectangular pores with rounded tips; (d-f) square array of elongated elliptical pores oriented to form a "X" pattern; and (g-i) square array of elongated elliptical pores oriented to form a zig-zag pattern. For all three geometries, we report a typical dispersion relation (a, d, and g), the evolution of the band gaps as function of the pores aspect ratio, a/b (b, e, and h) and the evolution of the band gaps as a function of the minimum ligament thickness, L_{\min} (c, f, and i).

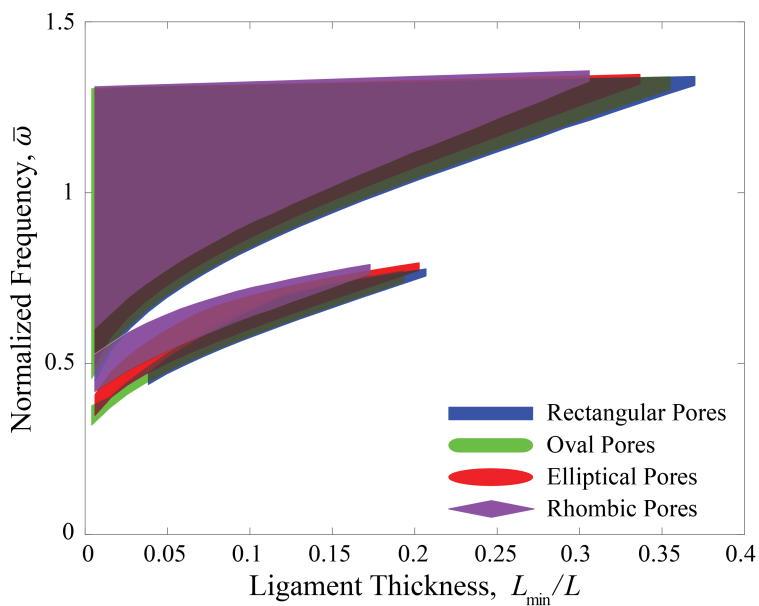


Figure S6: Effect of the pores profile on the band gaps in a square array of mutually orthogonal elongated pores with $\psi = 0.05$. The band gaps obtained for different pores profiles collapse on each other, confirming that the effect of the pores profile is minimal.

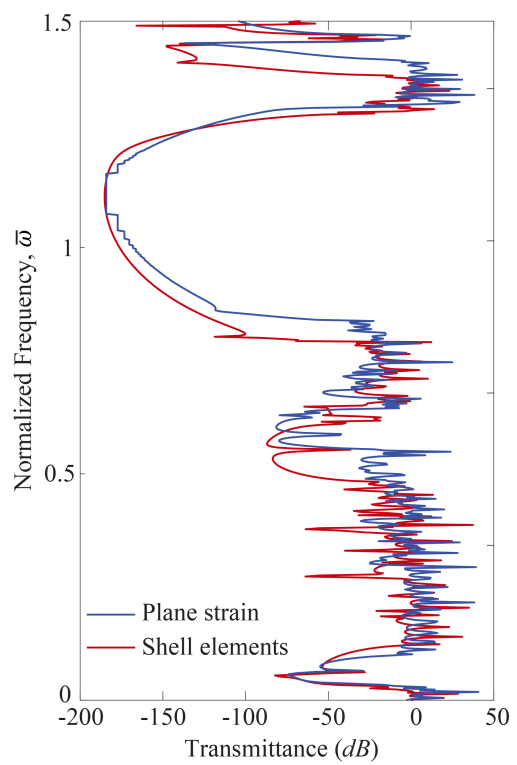


Figure S7: Transmittance of the proposed periodic structure made of the plane strain and shell elements.

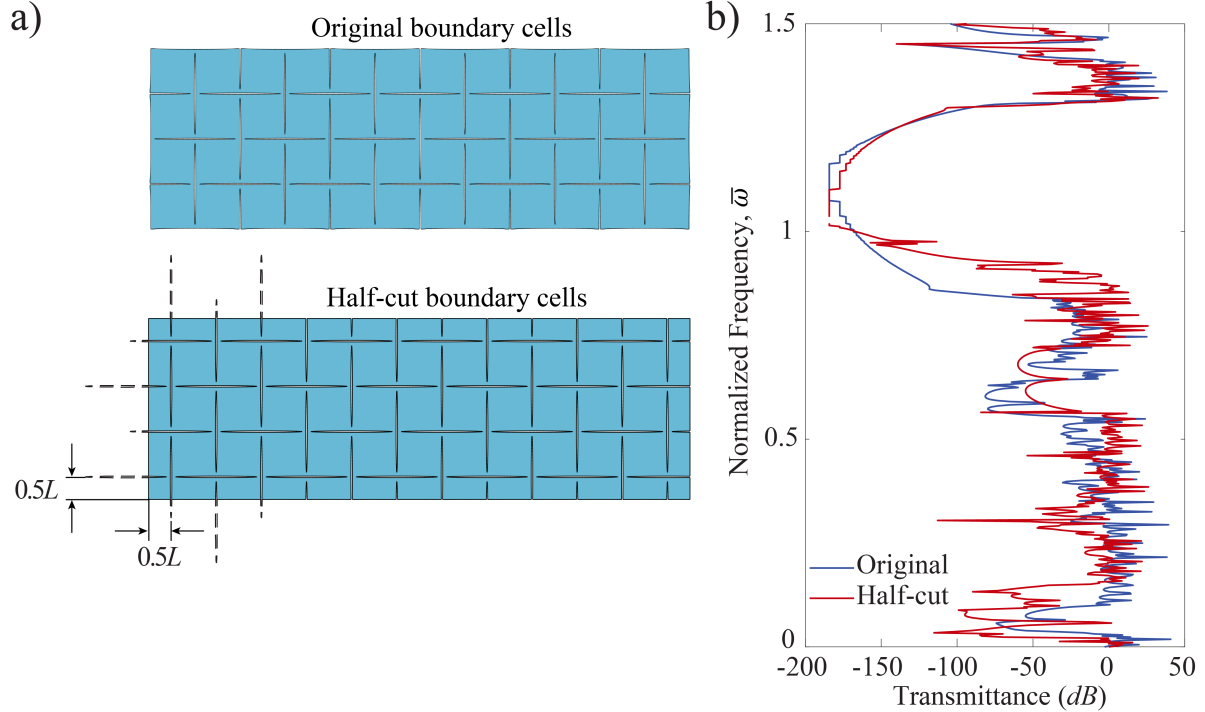


Figure S8: a) Finite-size models with different boundary cuts. b) Transmittance curves for the two models.

cuts (see Fig. S8a). Importantly, the transmittance curves shown in Fig. S8b indicate that the size and the location of the band gap remains almost unchanged in structures with different edge cuts.

Displacement and stress fields In Fig. S9 and S10, we show the displacement field and the von Mises stress distribution in the 6×2 structure at four different frequencies. The results reported in sections a, c, and d of Figs. S9 and S10, are for frequencies within the first, second, and the third bandgaps, respectively. As a result, the elastic energy in these cases is completely localized near the excitation site and no vibrations are transmitted to the opposite end of the sample. Differently, in section b of these two figures, we show the displacement and stress fields for a frequency out of the band gaps, so that the elastic waves are found to propagate through the structure.

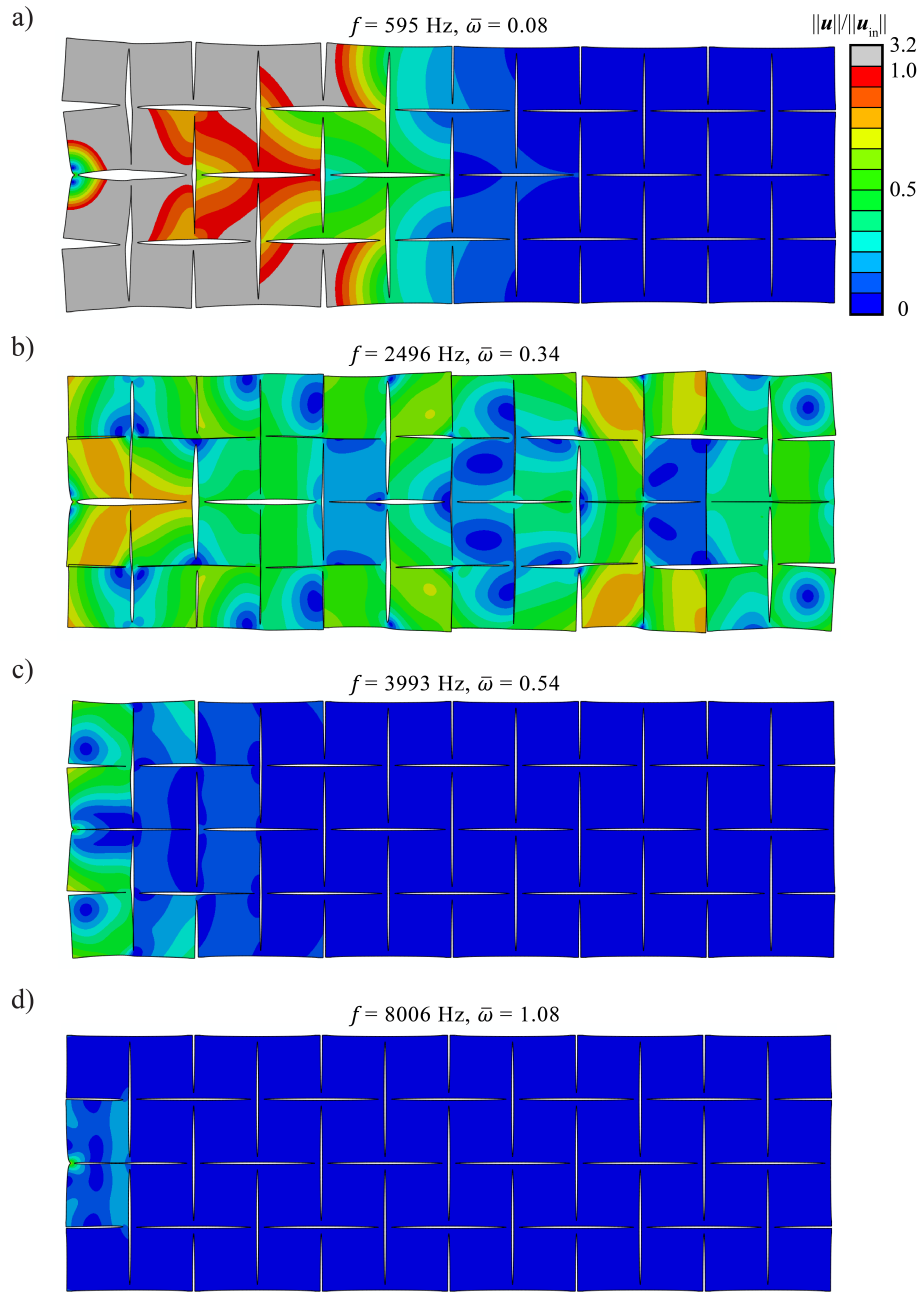


Figure S9: Displacement field distribution in finite-size structures comprising 6×2 unit cells at different frequencies: (a) $f = 595 \text{ Hz}$ (within the first band gap of the structure), (b) $f = 2496 \text{ Hz}$ (outside the band gaps), (c) $f = 3993 \text{ Hz}$ (within the second band gap of the structure), and (d) $f = 8006 \text{ Hz}$ (within the third band gap of the structure).

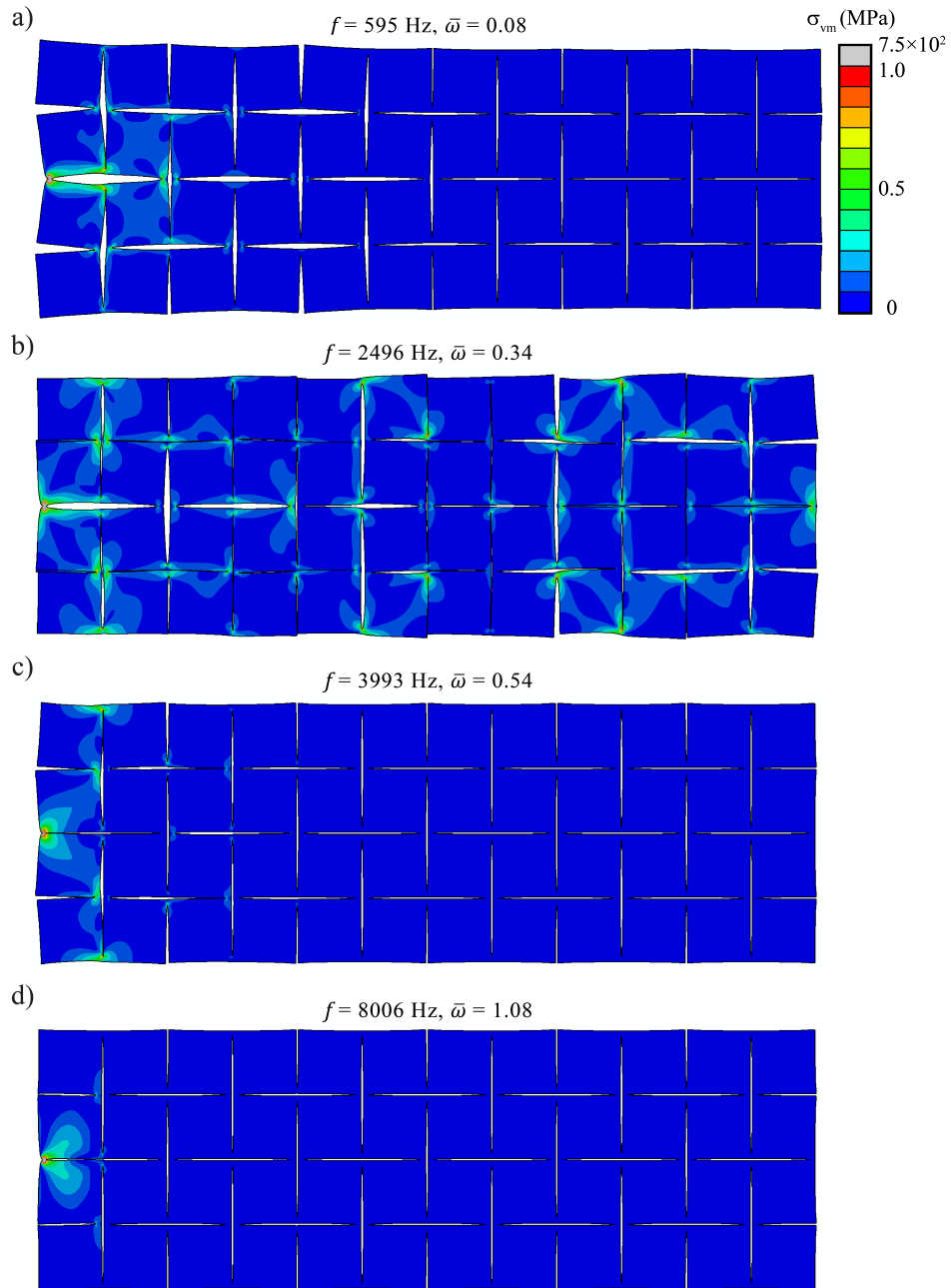


Figure S10: von Mises stress distribution in finite-size structures comprising 6×2 unit cells at different frequencies: (a) $f = 595 \text{ Hz}$ (within the first band gap of the structure), (b) $f = 2496 \text{ Hz}$ (outside the band gaps), (c) $f = 3993 \text{ Hz}$ (within the second band gap of the structure), and (d) $f = 8006 \text{ Hz}$ (within the third band gap of the structure).

1. Bloch, F. ber die quantenmechanik der elektronen in kristallgittern. *Zeitschrift fr Physik* **52**, 555–600 (1929).
2. Aberg, M. & Gudmundson, P. The usage of standard finite element codes for computation of dispersion relations in materials with periodic microstructure. *The Journal of the Acoustical Society of America* **102**, 2007–2013 (1997).
3. Wang, P., Shim, J. & Bertoldi, K. Effects of geometric and material non-linearities on the tunable response of phononic crystals. *Physical Review B* **88**, 014304 (2013).
4. Brillouin, L. *Wave Propagation in Periodic Structures* (McGraw-Hill, 1946).
5. Brillouin, L. *Wave Propagation and Group Velocity* (Academic Press, 1960).
6. Kittel, C. *Introduction to solid state physics* (Wiley, 2005).
7. Safavi-Naeini, A. H. & Painter, O. Design of optomechanical cavities and waveguides on a simultaneous bandgap phononic-photonic crystal slab. *Optic Express* **18**, 14926–14943 (2010).
8. Maldovan, M. & Thomas, E. Simultaneous complete elastic and electromagnetic band gaps in periodic structures. *Applied Physics B* **83**, 595–600 (2006).
9. Maldovan, M. & Thomas, E. *Periodic Materials and Interference Lithography for Photonics, Phononics and Mechanics* (Wiley-VCH, 2009).